J. Mol. Biol. (1995) **254**, 404–415

JMB

Lipid Location in Deoxycholate-treated Purple Membrane at 2.6 Å

N. Grigorieff[1]*, E. Beckmann[2] and F. Zemlin[2]

[1]*MRC Laboratory of Molecular Biology Hills Road, Cambridge CB2 2QH, UK*

[2]*Fritz-Haber-Institut der Max Planck Gesellschaft Faradayweg 4-6, 14195 Berlin, Germany*

**Corresponding author*

A high resolution projection at 2.6 Å of deoxycholate-treated purple membrane using only images has been obtained with a 200 keV FEG microscope operated at liquid helium temperature. Examination of this high quality map has allowed the following conclusions to be made: Comparison between the internal structure of the trimers of the native and the deoxycholate-treated crystal forms shows that almost every detail of the structure at high resolution is identical. The cell dimension change from 62.4 Å to 57.9 Å is accompanied by a loss of about half the normal lipids and a 2° anticlockwise rotation of the trimer as a rigid body. Three of the lipids per bacteriorhodopsin molecule remain in identical positions relative to the trimer. In addition, from the projection map together with a packing analysis using the atomic model for bacteriorhodopsin, space for three further lipids has been identified making a total of six lipids per bacteriorhodopsin molecule in this crystal form. Finally, the surprisingly small rotation of the trimer between the two crystal forms with completely different Van der Waals contacts suggest that the crystals are held together by strong, long-range electrostatic interactions.

Keywords: bacteriorhodopsin; purple membrane; lipid; 2-dimensional crystal; electron microscopy

Introduction

The light-driven proton pump bacteriorhodopsin (bR) is the only protein in the purple membrane (PM) of *Halobacterium halobium*. Its structure has been determined to 2.8 Å resolution in projection (Baldwin *et al*., 1988), and to 3.5 Å resolution in three dimensions (Henderson *et al*., 1990). The 3-D density map led to an atomic model for the protein and revealed the location of some of the lipids in the PM. The total number of lipid molecules associated with the three protein molecules per unit cell has been estimated to be between 21 and 40 (21, Kates *et al*., 1982; 32–33, Blaurock, 1975; 40, Blaurock & Stoeckenius, 1971) from a variety of chemical analyses, but the crystal structure suggests that there are about 30. About 70% of the lipids are phospholipids and 30% are glycolipids (Kates *et al*., 1982). The negatively charged head groups of the phospholipids on the intracellular surface (Henderson *et al*., 1978) account for most of the surface charge of the membrane (Szundi & Stoeckenius, 1987) and stabilise the arrangement of bR trimers in a hexagonal lattice (Sternberg *et al*., 1992). Replacement of the polar lipids by neutral lipids breaks up the hexagonal structure and notably slows down the photochemical cycle of the protein (Szundi & Stoeckenius, 1988). The preserved function and spectral characteristics of the protein in the neutral lipid environment suggests that there is little structural change in the protein but that the local pH due to the membrane surface charge is altered significantly (Szundi & Stoeckenius, 1987, 1988). The preservation of the bR conformation in a different lipid environment is also demonstrated by the structure of membranes after lipid depletion using deoxycholate (DOC), determined at 6.2 Å in projection (Glaeser *et al*., 1985) and at 6 Å in a 3-D study (Tsygannik & Baldwin, 1987).

In these lipid-depleted membranes about 60 to 70% of the lipids were extracted. This was measured by lipid extraction and calculation of the remaining area in projection occupied by lipids. The lipid-depleted membranes maintained their hexagonal lattice with a reduction of the lattice constant from 62.4 Å to 57.3 Å. Also, in the early work, there was no apparent change in the trimeric arrangement of

Abbreviations used: FEG, field emission gun; bR, bacteriohodopsin; PM, purple membrane; DOC, deoxycholate; CTF, contrast transfer function; IQ, signal-to-background ratio on a scale of 1 to 9 (Table 1); 3-D, three dimensional.

0022–2836/95/480404–12 $12.00/0

the bR molecules or the orientation of trimers in the lattice. Geometric considerations led to the conclusion that the remaining lipids must be located at the 3-fold axis in the centre of the trimer and at the 3-fold axes between the trimers.

In this work we focus on the nature of the trigonal crystals of bR and how the trimers fit together in both the natural and the lipid-depleted *p*3 crystal forms. The position of lipids and changes in the orientation of the bR trimer in DOC PM are compared to native PM. With the precise determination of the cell dimensions and position of the trimer in the unit cell of DOC-treated membranes the space for the remaining lipids has been accurately located.

Results and Discussion

Quality of images

The projection structure of DOC bR at 2.6 Å in ice is shown in Figure 1(a) together with the projection structure of native bR at 2.8 Å in glucose (Baldwin *et al*., 1988) in Figure 1(b). The 3-fold axes in Figure 1(a) are labelled with Roman figures according to Tsygannik & Baldwin (1987). The two structures are identical in almost every detail. Local differences may be accounted for by errors in the phases and amplitudes in both maps as well as the different embedding medium. Since no high resolution electron diffraction data for DOC PM are available because the membranes are too small, the image amplitudes were scaled in resolution zones against diffraction data from the native form following the procedure given by Schertler *et al*. (1993). Figure 2 shows plots of the fall-off in image amplitudes in resolution zones for DOC PM to 2.6 Å and for native PM to 2.8 Å, using native PM electron diffraction amplitudes for the comparison.

Image and electron diffraction amplitudes depend on the degree of crystalline order of the sample. Disorder (displacement of unit cells from their crystallographic position) reduces amplitudes in both cases as the resolution increases (Grigorieff & Henderson, 1995). For native PM, observed diffraction amplitudes at 4 Å measured by electron diffraction are reduced to about 70% of their expected value for a perfectly ordered structure, due to disorder. At higher resolution amplitudes also fade faster due to beam damage in the sample.

Image amplitudes suffer further attenuation when the specimen or the image moves during exposure due to instabilities in the cold stage, beam damage and charging of the sample (Henderson, 1992). The precise dependence of image amplitudes on these parameters is still not fully understood. Finally, image amplitudes also depend on the contrast transfer function (CTF) of the microscope. Apart from the oscillation of the CTF *versus* resolution there is also an envelope function which attenuates the CTF at higher resolution. The envelope causes an additional reduction of amplitudes and depends on the energy of the electron beam, its spatial and temporal coherence and the defocus (Wade, 1992). The use of a field emitter as an electron source improves both spatial and temporal coherence over that found for tungsten filaments. For native PM, image amplitudes were about 8% of their corresponding electron diffraction amplitudes at 4 Å, with a defocus of about 4000 Å, 120 keV electrons and a tungsten filament (Figure 2 and Baldwin *et al*., 1988). With a hot field emitter and 200 keV these amplitudes go up to about 16% for DOC PM (Figure 2) in the present work. The coherence of the FEG source clearly produces a great improvement. It is also possible that part of the improvement is due to increased order in the crystals after removal of some of the lipids.

Following the procedure used for analysis of the accuracy of the native 2.8 Å data (Baldwin *et al*., 1988) the DOC data were divided into two data sets containing approximately the same amount of information. Averaged phases from each set were compared with one another and phase residuals calculated. These are shown in Figure 3 together with the estimated errors for the averaged phases from the complete data set. The phase difference between the two halves of the data increases towards higher resolution but stays below 80° to 2.6 Å confirming the estimated resolution. The estimated phase error, given by the continuous line in Figure 3, is better than 40° over the entire resolution range. Phase residuals and estimated errors do not increase monotonically with resolution. Since only seven images were included in the analysis these fluctuations may be statistical.

The signal attainable for a given image at high resolution depends on the removal of image distortions (unbending) by image processing. An important parameter is the size of the reference area which is used to find the exact positions of unit cells across the image. In this work the size of the area was chosen to include about 14 unit cells. A reference area of this size allows removal of distortions over distances of four unit cells or longer. Displacements of individual unit cells (trimers in this case) from the smoothed lattice positions remain undetected, however. Random displacements of individual trimers by about 0.5 Å are expected in native PM from a study of the diffuse background in electron diffraction patterns (Grigorieff & Henderson, 1995). Thus, in the case of PM, resolution is currently not significantly limited by the intrinsic disorder in the crystals although the strength of the diffraction spots would be greater if there was less disorder. In some other crystals a signal is only detectable at considerably lower resolution (e.g. rhodopsin at 9 Å, Schertler *et al*., 1993; light-harvesting complex I at 8.5 Å, Karrasch *et al*., 1995; halorhodopsin at 6.0 Å, Havelka *et al*., 1993). Since resolution degrading mechanisms such as contrast in the microscope, beam damage and sample movement for all these specimens are probably very similar to those for PM, it is likely that the limited resolution with these other crystals is due to short range disorder which cannot be

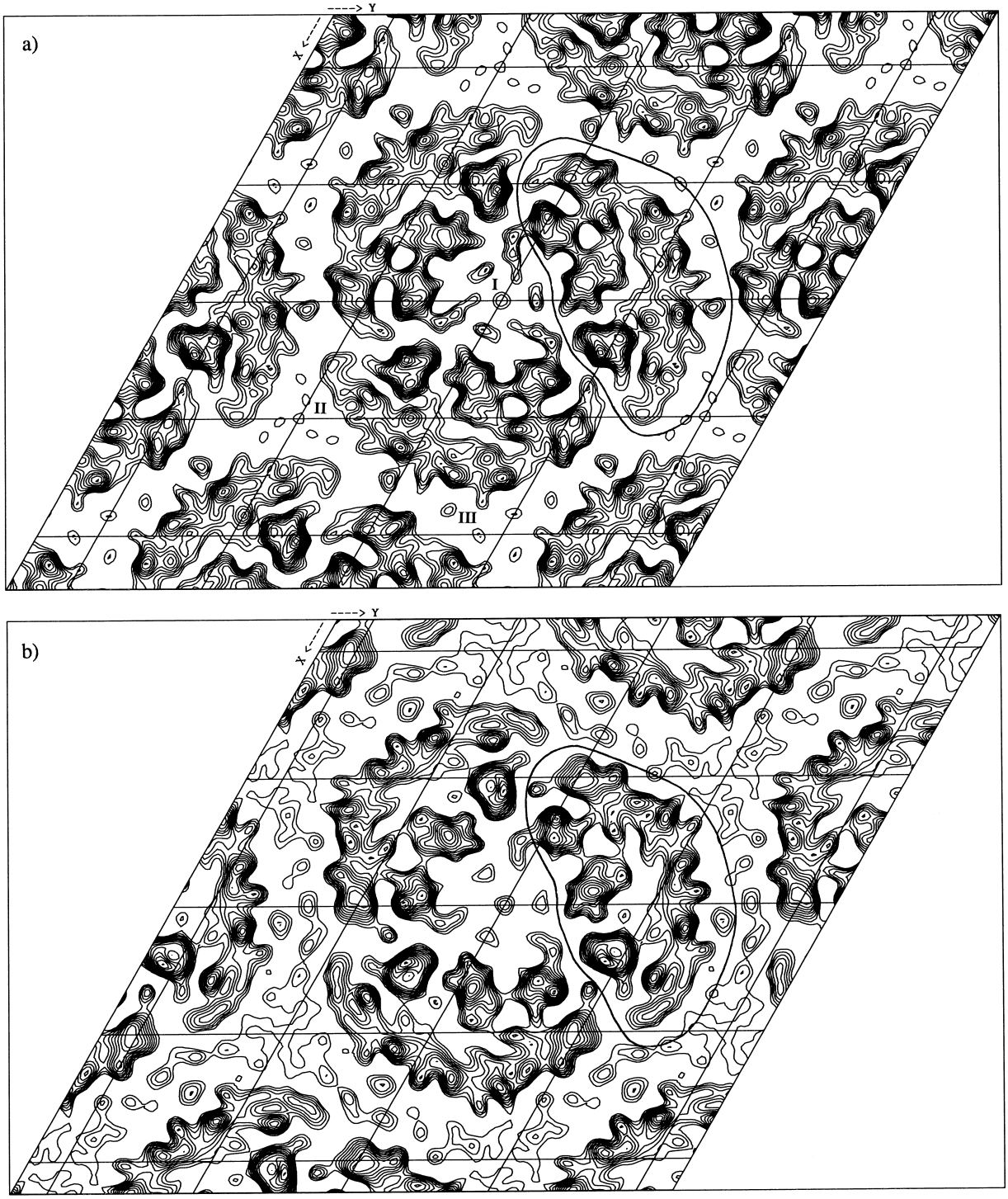

Figure 1. (a) Projection map of DOC-treated PM at 2.6 Å and (b) native PM at 2.8 Å. The 3-fold axes in (a) are labelled with Roman figures. One bR molecule is outlined in each map.

removed with a large reference area. The disorder may include rotational misalignment which is not corrected for in the present procedure. If the short range disorder could also be removed the attainable resolution is likely to be significantly extended. Therefore, it is interesting to see if the images recorded in this work allow determination of the positions of individual trimers which form a rigid unit (Grigorieff & Henderson, 1995). One of the images was digitised over a larger area (9900×9900 pixels) and at slightly higher resolution (0.77 Å per pixel giving 1.5 Å resolution cut-off). A CTF plot for this image is shown in Figure 4 and IQ values are listed in Table 1. Table 2 shows the signal-to-background ratio, after background subtraction, between 3 and 4 Å for different sizes of a reference

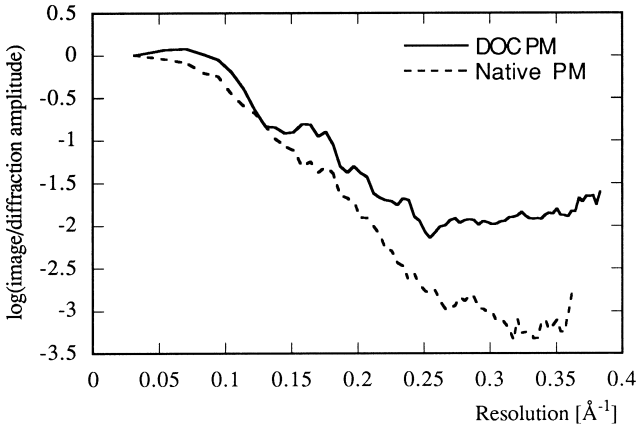

Figure 2. Ratio of image amplitudes (DOC PM, continuous line; native PM, dotted line) and electron diffraction amplitudes *versus* resolution. The electron diffraction data were collected from native PM.

area. Each reference area was derived from the original image after one pass of unbending (300×300 pixel reference area) and Fourier averaging. Before unbending, Fourier averaging was also applied to the image with hole sizes in the Fourier mask depending on the size of the reference area. When the image was unbent using only one trimer as a reference area, no Fourier averaging was applied and the whole unit cell was searched for cross-correlation peaks. Thus, in this case, no advantage was taken of the fact that the protein trimers were arranged in a 2-D crystal lattice. There is a maximum of about 41/7 for a reference area of 14 unit cells. For a larger reference area the signal is smaller as the determination of unit cell positions is less sensitive to distortions on a smaller scale. When the reference area is smaller than 14 unit cells noise becomes more dominant and the signal is limited by the accuracy with which unit cell positions can be determined. But even for a reference area of just one unit cell the signal-to-background ratio is still better than 4/7. This is an important result for the future development of image processing. It shows that it is possible, at least in two dimensions, to align particles of the size of the trimer of bR (about 90 kDa including some lipids) so that significant Fourier power can still be detected at 3 Å resolution. More sophisticated image processing software should, in principle, be able to take advantage of this and bring structures currently only resolved at comparatively low resolution up to a resolution similar to that for bR.

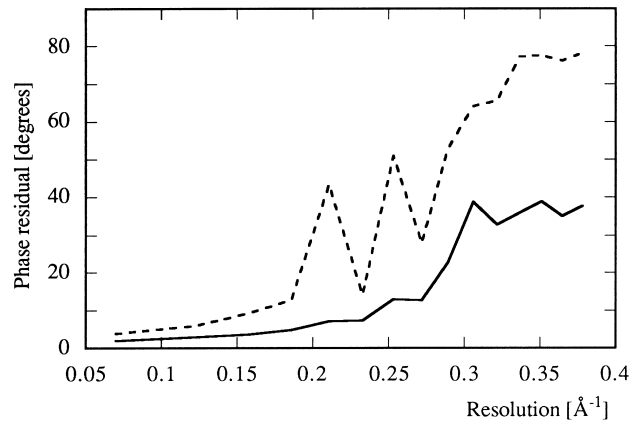

Figure 3. Estimated phase errors in resolution zones. The dotted line shows phase residuals between two halves of data with roughly equal information content. The continuous line plots phase error estimates for the final averaged data. For both plots random data would give a 90° phase residual.

Rotation of the trimer and lattice constant

The reduction in unit cell size of the DOC-treated membranes is readily seen from the reduced space between the trimers compared with that in native PM. A more detailed inspection of the two maps shows there is no significant difference between the trimers suggesting the structure of the trimers is identical. A careful comparison yields a small anti-clockwise rotation of the trimer in DOC PM with respect to that in native PM. The precise rotation angle was measured to be 2.03° by cross-correlation of the trimers from each crystal form.

The unit cell size of the DOC PM was determined (1) by X-ray diffraction of pelleted membranes (the X-ray diffraction pattern was calibrated against a pattern from native PM), (2) by electron diffraction (calibration of the electron diffraction pattern was done against polycrystalline cubic ice; Dubochet *et al*., 1982), and (3) by cross-correlation of the trimer with the native form. The cross-correlation between the trimers from each crystal form was calculated for a series of magnification factors and rotation angles. The correlation map (not shown) has a well-defined maximum at a unit cell size of 57.9 Å and a rotation of $-2.03°$. Results are summarised in Table 3 and are in good agreement with Glaeser *et al*. (1985) and Tsygannik & Baldwin (1987). In the following we will use an averaged value of 57.9 Å for the cell dimensions of DOC PM compared with 62.4 Å for native PM.

For native PM the total area of lipid was assumed to be 32% or 1080 Å^2 of the unit cell (Engelman *et al*., 1980). The unit cell area is reduced upon treatment with DOC by 470 Å^2 leaving 610 Å^2 or 21% of the unit cell for the remaining lipid. Assuming 30 lipid molecules per unit cell in the native form an area of 610 Å^2 gives space for 17 lipids or 56% of the original lipid content.

Difference between glucose and water-embedded membranes

The work by Glaeser *et al*. (1985) and Tsygannik & Baldwin (1987) was carried out with membranes embedded in glucose. The image data from this work (ice-embedded membranes) gives *R*-factors of 16% and 19%, and phase residuals of 25° and 32° against the 6.2 Å data of Glaeser *et al*. (1985) and

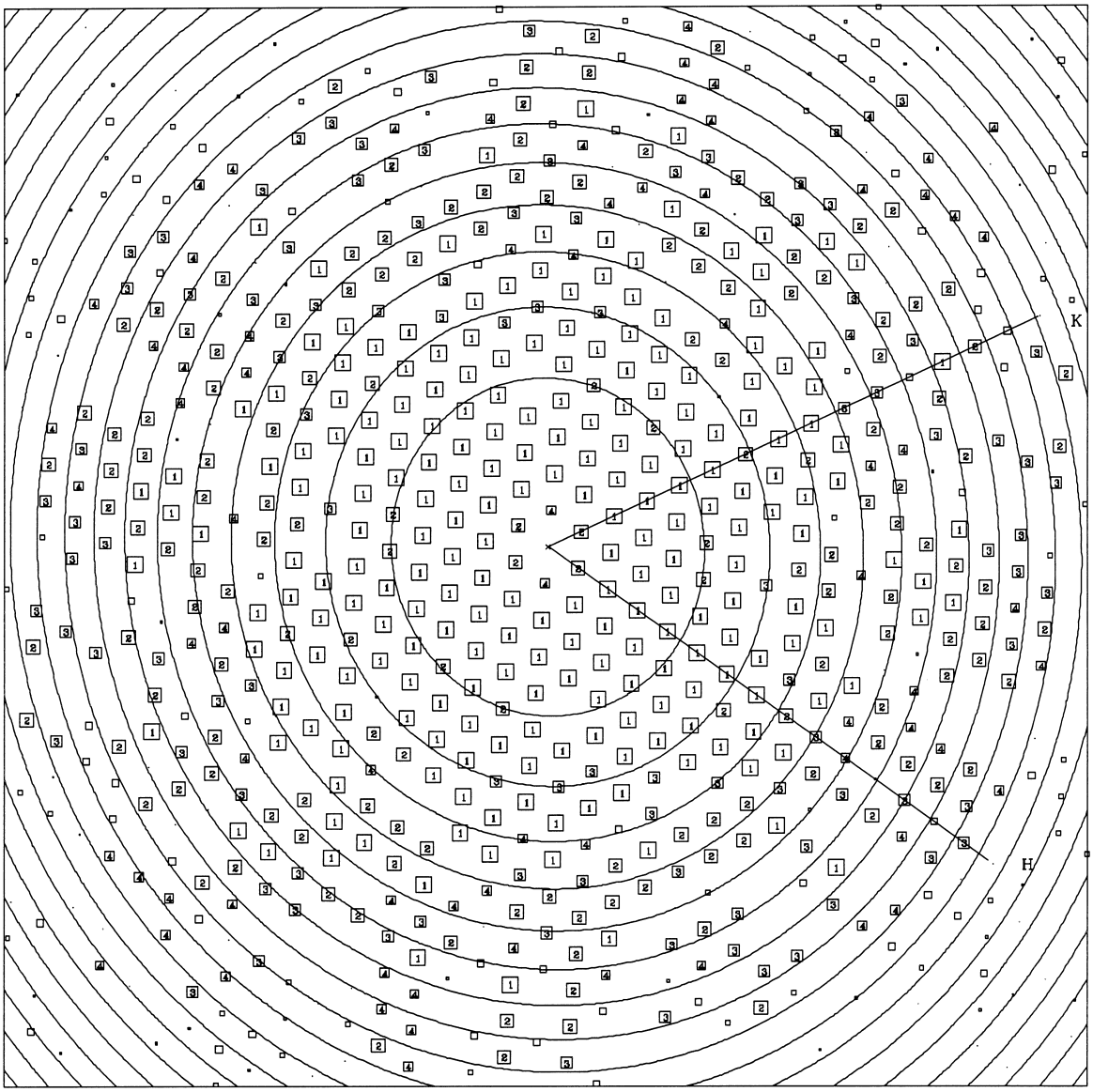

Figure 4. CTF plot for a 9900 × 9900 pixel image containing 140 × 140 unit cells. The plot boundaries are at 3.3 Å.

the 6.0 Å data of Tsygannik & Baldwin (1987), respectively. The density of glucose is about 50% higher than that of ice (see Table 4), and a difference map between glucose and ice-embedded samples can, therefore, provide some information about the surface topology of the membrane. A difference

Table 1. The IQ values in resolution zones for a 9900 × 9900 pixel image containing 140 × 140 unit cells

Resolution (Å)	IQ = 1 (S/B > 7)	2 (7.0–3.5)	3 (3.5–2.3)	4 (2.3–1.8)	5 (1.8–1.4)	6 (1.4–1.2)	7 (1.2–1.0)	8 (1.0–0)	9 (< 0)	All
∞–7.0	72	11	5	1	0	0	1	3	0	93
7.0–5.5	24	13	5	4	2	1	0	4	4	57
5.5–4.5	11	24	9	11	2	2	4	10	2	75
4.5–4.0	8	17	9	5	6	0	2	8	11	66
4.0–3.5	0	10	14	10	13	5	0	10	19	81
3.5–3.2	0	3	4	5	5	10	4	20	21	72
3.2–3.0	0	0	0	2	6	9	6	23	23	69
3.0–2.8	0	0	1	3	3	5	6	17	31	66
2.8–2.7	0	0	0	0	2	1	2	15	31	51
2.7–2.6	0	0	0	1	2	4	4	9	22	42
∞–2.6	115	78	47	42	41	37	29	119	164	672

The IQ equivalent signal-to-background ratio (S/B) after subtraction of the background is given in brackets.

Table 2. Average signal-to-background ratio of all spot intensities in the resolution range 3.0 Å to 4.0 Å, obtained for one image using different reference areas to find the position of unit cells

Area in pixel	Unit cells	% Fourier averaging	Reflections found with IQ $\leqslant$ 7	Signal/Background
300 × 300	73	99	79	10/7
200 × 200	33	98	88	25/7
130 × 130	14	91	107	41/7
70 × 70	4	80	100	37/7
34 × 34	1	0	70	4/7
Unprocessed image			40	0/7

In each case, Fourier averaging was applied to the image before unbending except in the last two rows. The value (in %) in the third column refers to the area masked out by the Fourier mask applied to the image transform. The signal-to-background ratio was calculated after subtraction of the background from each integrated spot intensity. The total number of reflections in the chosen range was 222. The signal refers to the average intensity above background at the position expected for the diffraction peaks from the crystal. The background is the average intensity in the immediately surrounding area; it is normalized to 7. The standard deviation of the background is the background fluctuation after the intensity of all reflections has been averaged. It was determined to be 1.0 for the single molecule cross-correlation in the second last row. Thus, a peak of 4 is above a background of 7 by 4× the standard deviation. The signal-to-background ratio for the unprocessed image was included for comparison in the last row.

map at 6.2 Å shown in Figure 5 was calculated between the data published by Glaeser *et al*. (1985) and data from this work. The map indicates positive density mainly at the 3-fold axes and negative density predominantly in areas filled by protein. This could be due to either a difference in the distribution of the embedding material, or a protrusion of the protein from the membrane which leaves space in the lipid areas to be filled up by the embedding material. The second interpretation was also put forward by Zaccai & Gilmore (1979) who collected neutron diffraction data from native PM with the hydrogen in H_2O replaced by the deuterium in ^2H_2O to locate hydration sites. They calculated the overall height of the bR molecule above the lipid to be 1.5 Å. A similar calculation can be done here when we consider the mean densities of protein and lipid in the projection maps from glucose and ice-embedded membranes. These are given in Table 5 for projection maps in arbitrary units scaled so that the average density is zero and the maximum density is 250. The values were calculated assuming areas of protein and lipid of 2293 Å^2 and 610 Å^2, respectively. Given an average thickness of the protein of 45 Å (Henderson & Unwin, 1975) and using the relative densities for protein, lipid, glucose and ice given in Table 4 as their inner potentials, the average projected densities were calculated in each case. The mean thickness for the glucose layer was determined to be 1.3 Å (Glaeser *et al*., 1985) and 1.7 Å (Tsygannik & Baldwin, 1987). This is in good agreement with the thickness of 1.5 Å given by Zaccai & Gilmore (1979) as well as Henderson (1975) who gave an upper limit of protrusion of the protein above the lipid level of 7 Å. The estimate of 7 Å was calculated from changes of low order reflections in X-ray diffraction upon variation of the density of the embedding medium.

The highest peak in the difference map in Figure 5 is found at 3-fold axis III suggesting there is a lipid-free hole extending part of the way through the membrane at that location. In the following section it will be shown that there is little room for lipid at this 3-fold axis and that the remaining space might, therefore, be filled by the embedding medium.

Table 3. Measured lattice parameters for DOC-treated PM

Method	Lattice parameters (Å)
Electron diffraction	57.6 ± 0.6
X-ray diffraction	58.0 ± 0.3
Cross-correlation with native PM	57.9 ± 0.1

Location of lipids

The measurement of cell dimensions and rotation of the trimer allows the exact position of the current model for bR (Henderson *et al*., 1990) in the unit cell of DOC-treated PM. Phases calculated from the repositioned model give an average phase residual of 47° to a resolution of 3.3 Å when compared with

Table 4. Mass density and inner potential for various materials

Material	Mass density (g/cm^3)	Inner potential (V)
Water	1.0	4.9
Ice	0.93[a]	4.5
Lipid	1.0[b]	6.5
Protein	1.32[c]	8.3
Glucose	1.56[d]	8.3

The inner potential was calculated from the mass density, molecular weight and scattering power for one molecule. The scattering power (not listed) was estimated from the sum of atomic scattering factors (International Tables of Crystallography, 1992) for each atom in the molecule.

[a] Dubochet *et al*. (1988).
[b] Tanford *et al*. (1974).
[c] Blaurock *et al*. (1975).
[d] CRC Handbook of Chemistry and Physics (1978).

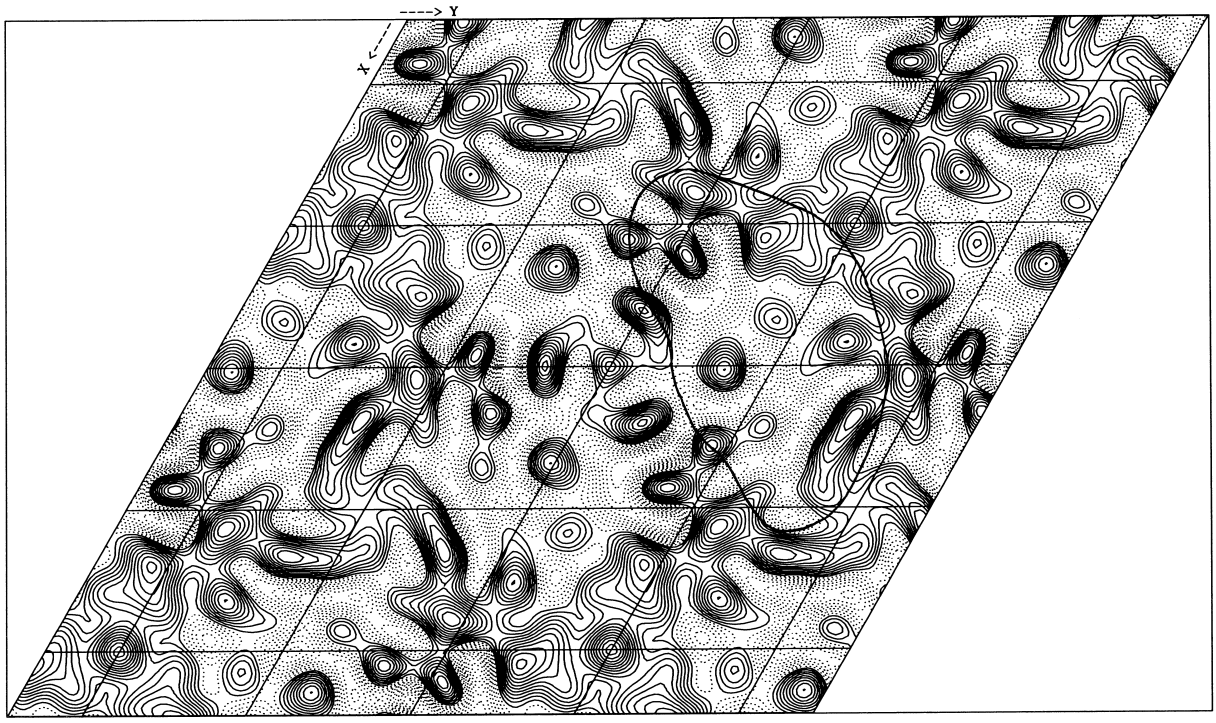

Figure 5. Difference map at 6.2 Å, calculated from the vectorial difference between structure factors for glucose-embedded membranes (Glaeser *et al*., 1985) and ice-embedded membranes (this work). The outline of one bR molecule is indicated.

the new projection image data from DOC PM, indicating good agreement between the model and the measured data. A 3-D density map was calculated from the model and 15 Å thick slices through this map on the intracellular and the extracellular side are shown in Figure 6(a) and (b), respectively. Possible locations for lipid molecules are indicated for both sides of the membrane. The total number of lipids indicated is 18 (6 unique lipid molecules with 12 symmetry-related) which agrees well with the remaining lipid calculated above from the reduction of available area. Lipids 1 and 4 on each side of the membrane in the centre of the trimer coincide with lipid locations in native PM. Although it is less obvious, there is also space for lipid 2 on the intracellular side. In native PM there is clear density for this lipid in the experimental 3-D map (Henderson *et al*., 1990) buried in a crevice between two bR molecules. The density can accommodate one tail of lipid 2 and suggests that the second tail is on the outside of the trimer. The neutral lipid squalene, an alternative occupant for the density with a concentration of two molecules per unit cell in native PM (Kates *et al*., 1982), has a 50% longer chain length and was found to be too long to fit into the space. Since there is no evidence of a change of structure of the trimer and space for the second tail on the outside of the trimer is also present in the DOC-treated PM (Figure 6(a)), it is likely that lipid 2 remains in the membrane. Lipid 3 and symmetry-related molecules, possibly poorly ordered on the intracellular side, must fill remaining space at 3-fold axis II.

At 3-fold axis III no lipids are indicated in Figure 6(a) and (b) but there appears to be space for a single lipid on the intracellular side. It is possible that the space is void of lipid and filled with ice as suggested by a peak in the difference map in Figure 5 between glucose and ice-embedded membranes (see above). The idea of small gaps in DOC-treated membranes is also supported by a study of negatively stained membranes where it was found that contrast is slightly higher for

Table 5. Measured average projected densities of protein and lipid in glucose and ice-embedded membranes

	Glaeser *et al*. (1985)	Tsygannik & Baldwin (1987)	This work
Embedding material	Glucose	Glucose	Ice
Protein density (arbitrary units[a])	17.9	17.3	18.5
Lipid density (arbitrary units[a])	–60.5	–59.4	–64.9

[a] All maps were scaled to have a maximum of 250 and an average of 0.

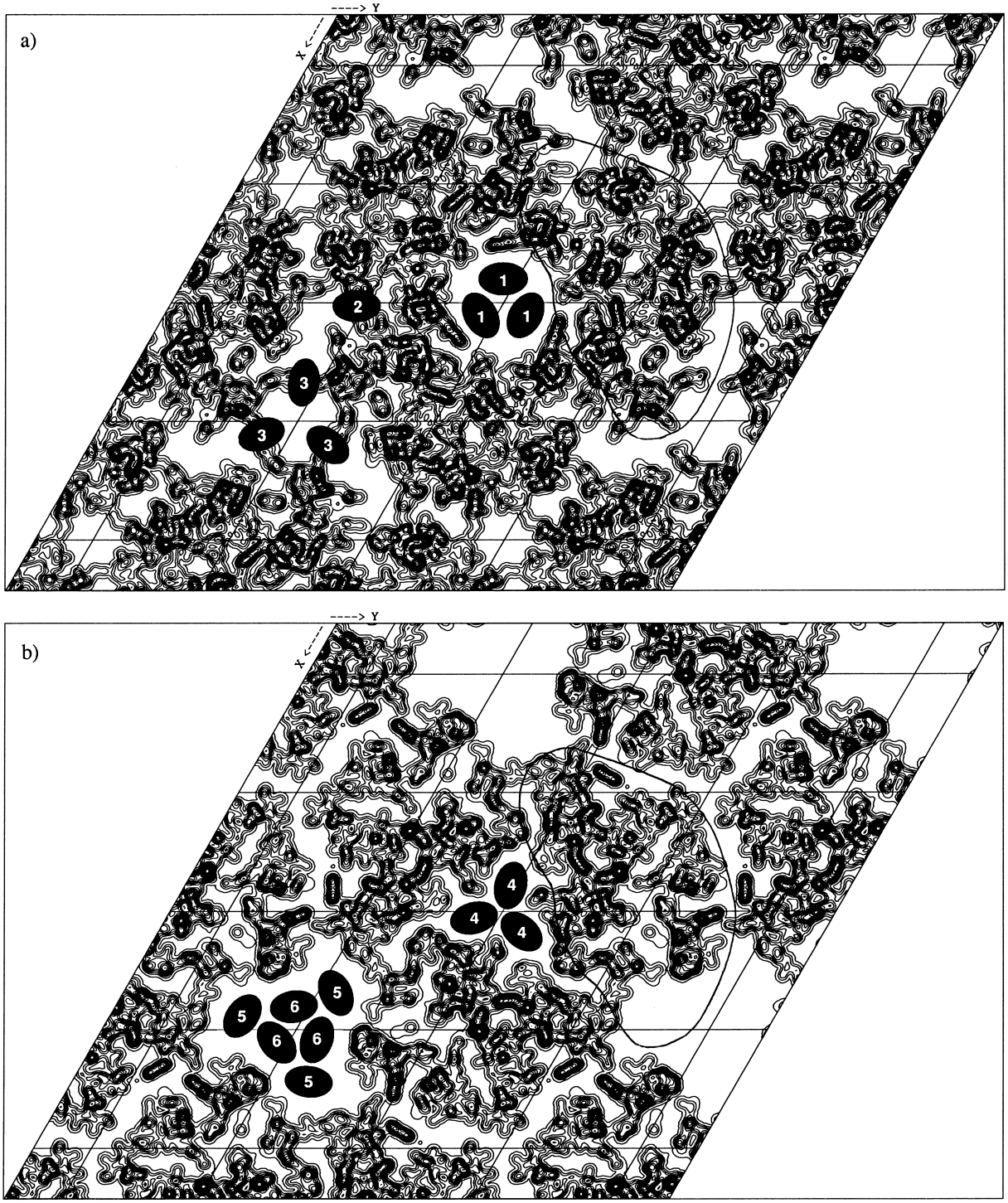

Figure 6. 15 Å thick slices through a calculated 3-D density map parallel to the membrane surface. The map was calculated from the current bR model for native PM with the bR trimer repositioned in the DOC unit cell. Lipids likely to be present after DOC treatment are indicated by ovals. (a) density on the intracellular and (b) density on the extracellular side. One bR molecule is outlined in each map.

DOC-treated PM than it is for native PM (Hwang & Stoeckenius, 1977).

On the extracellular side there is no space at all for lipid at 3-fold axis III. Lipids 5 and 6, possibly disordered, must fill space at 3-fold axis II on the extracellular side.

Table 6 summarises the number of possible lipid molecules at each 3-fold axis. In the current atomic model for native bR there is space for 30 lipid molecules, and all positions equivalent to the lipid positions indicated in Figure 6(a) and (b) are assumed to be occupied by lipid. Table 7 lists those

Table 6. Number of lipids in DOC-treated PM at 3-fold axes and between bR monomers

Surface	Number of lipids at 3-fold axis I	II	III	Lipids between bR monomers	Total per unit cell
Intracellular	3	3	0 or 1	3	9 or 10
Extracellular	3	6	0	0	9
Total	6	9	0 or 1	3	18 or 19

lipids which are resolved in the 3-D map of native PM.

Thus, possible locations for 18 or 19 lipid molecules per unit cell can be identified by considering the remaining space in DOC-treated PM.

Glaeser *et al*. (1985) and Tsygannik & Baldwin (1987) found space only for 12 lipids and 12 to 14 lipids per unit cell, respectively. The difference may be accounted for by a slightly larger lattice parameter determined in this work (57.9 Å instead of 57.3 Å) and an additional lipid position (lipid 2 in Figure 6(a)) now identified between the bR monomers. Also, the space for six lipids at 3-fold axis II on the extracellular side is not visible in projection because of the tilting of the α-helices and, therefore, it was not considered by Glaeser *et al*. (1985) who concluded there was no lipid at this position. Tsygannik & Baldwin (1987) assumed three lipids at this location based on their 3-D map at 6 Å which includes an uncertainty in the size of the side-chains. However, they allowed space for a further three lipid molecules on the extracellular side at 3-fold axis III where our study concludes there is not enough space for lipid. They find space for only 0 or one lipid at 3-fold axis II and III on the intracellular side where this study shows space for three lipids at 3-fold axis II.

It is worth noting that the density between the trimers seen in projection in Figure 1(a) can be misleading in the determination of the location of lipid molecules. For example, at 3-fold axis III there are six peaks which could be interpreted as density from ordered lipid molecules. But inspection of the atomic model (Figure 6(a) and (b)) reveals that the density must be due to protein. On the other hand the remaining lipid can be reliably estimated from the reduction in unit cell area provided the amount of lipid in the native form is known accurately.

Trimer orientation

The small rotation of the trimer between the two crystal forms with completely different Van der Waals contracts between trimers suggests that the crystals are held together by strong, long-range electrostatic interactions which maintain trimer orientation in the two forms. This idea is supported by a major change in the order of the lattice upon treatment of PM with 0.5 M HCl (Henderson *et al*., 1982). A pH of 0.5 in this solution is sufficient to protonate most of the acidic surface residues of bR and, thus, change the electrostatic potential. It was found that this results in a 10° anticlockwise rotation of the trimer.

It is difficult to evaluate exactly the electrostatic potential and forces acting between trimers in the membrane because the local dielectric constants of protein, lipid and embedding medium are not known. Also, the positions of the charged lipid head groups are only certain to within 10 Å or so. Finally, some ionisable residues in the protein may not be fully ionised or their charge may be screened by surrounding ordered water molecules. But we may hope that gross features on a plot of the electrostatic potential produced by charges on ionisable side-chains give some indication of the preferred orientation of the trimers to each other. Plots of the projected potential in 10 Å thick slices are shown in Figure 7(a) for the intracellular side and in Figure 7(b) for the extracellular side. Since most charges are located near the surfaces of the membrane, the potential in the middle of the molecule is less important for the orientation of the trimer, and it is not shown here. The scale of the plots in Figure 7(a) and (b) is the same as in Figure 1(a) but adjacent trimers are not included in the calculation. Dotted lines indicate a negative potential whereas continuous lines indicate a positive potential. In these plots it was assumed that all lysine, arginine, aspartic and glutamic acid

Table 7. Resolved density in the three-dimensional map of native PM for lipid molecules in positions indicated in Figure 6(a) and (b) for DOC-treated PM

Lipid position in DOC PM	Lipid in 3D map of native PM
1 (top, centre of trimer)	Not resolved
2 (top, crevice between monomers)	Resolved
3 (top, 3-fold axis II)	Not resolved
4 (bottom, centre of trimer)	Resolved
5 (bottom, 3-fold axis II)	Not resolved
6 (bottom, 3-fold axis II)	Resolved

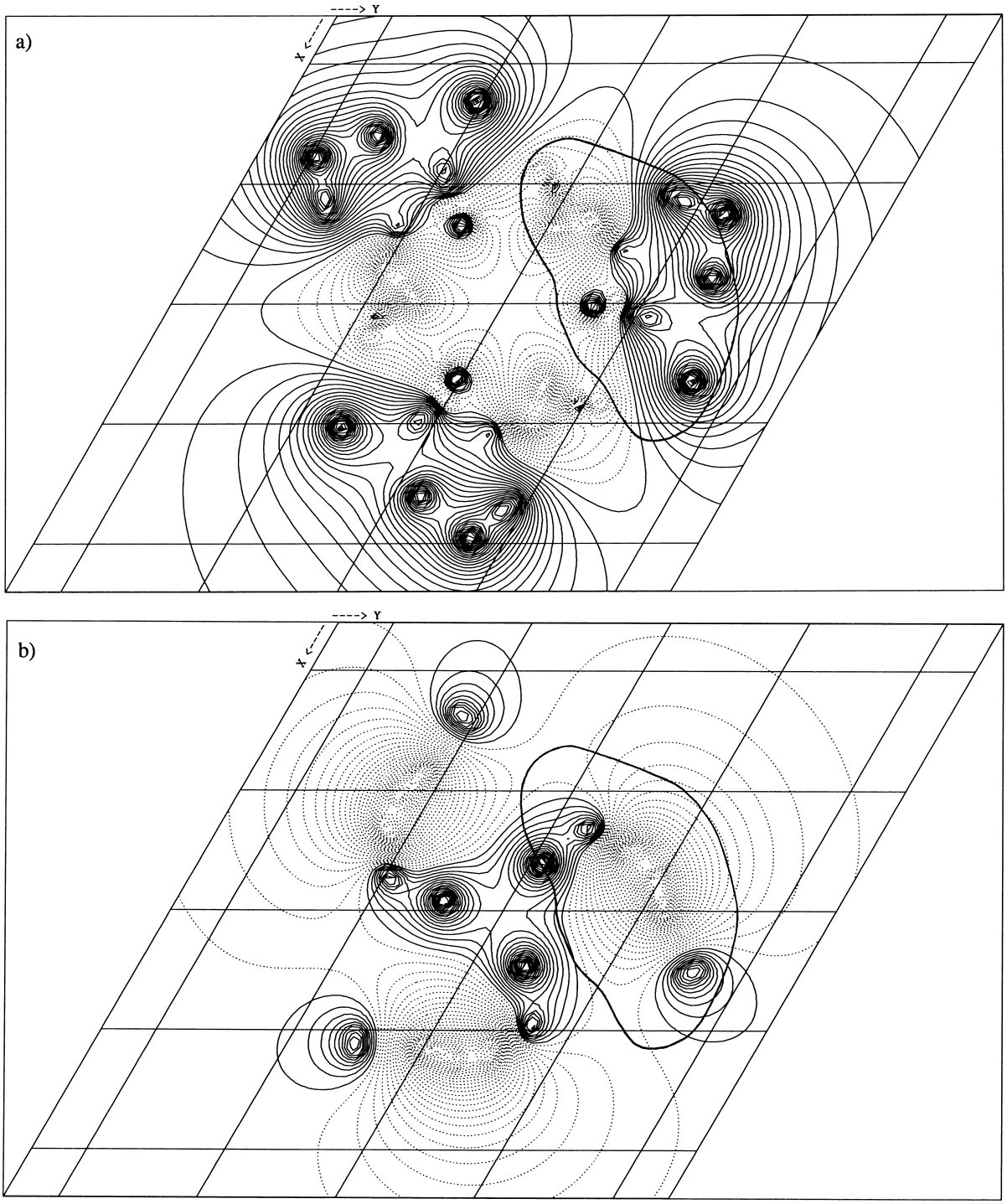

Figure 7. Plots of the projected Coulomb potential of one trimer in 10 Å slices (a) on the intracellular side and (b) on the extracellular side, produced by charged residues in the bR molecule. A constant dielectric constant was assumed and the effect of surrounding lipid was ignored. Dotted lines indicate a negative potential whereas continuous lines indicate a positive potential. One bR molecule is outlined in each map.

side-chains are fully ionised and that the surrounding volume has a uniform dielectric constant. There are more charged residues on the intracellular than on the extracellular side. The potential on the intracellular side of the membrane seems to form a large negative triangular area in the middle of the trimer and positive lobes outside the trimer along the sides of the negative triangle. The corners of the triangle point towards adjacent trimers (not shown) where they make contact with negative lobes. Thus, on the intracellular side, the orientation of the trimers brings negative charges in close contact with positive charges, as expected from electrostatics. On the extracellular side there is a concentration

of positive charge in the middle of the trimer surrounded by areas of alternating positive and negative potential. The orientation of this circle of alternating positive and negative potential deviates by about 10° from a perfect alignment where the distances of charges of opposite sign are minimised. From this it seems the two sides of the trimer prefer slightly different orientations and compete to minimise their local potential energies. Since the two sides are rigidly connected the final orientation of the trimer will correspond to a minimum in the overall potential energy. Due to the larger magnitude of the potential on the intracellular side the orientation of the trimer is likely to be determined mainly by the charge distribution on that side. Thus, the overall charge distribution and the small observed change in orientation of the trimer in DOC PM are in agreement with the view that electrostatic forces are a major factor in the packing of trimers both in DOC-treated and native PM.

Conclusions

Careful analysis of the highest resolution projection structure of a protein so far obtained by electron microscopy has shown the structure of the trimer in deoxycholate-treated purple membrane is almost indistinguishable from that in the native membrane. A small 2° anticlockwise rotation was accurately measured and the positions of six lipids were deduced. Finally, in view of future development, the excellent image quality demonstrated the possibility of atomic resolution structure determination also from poorly ordered crystals by single molecule analysis.

Materials and Methods

The lipid extraction procedure followed that given by Glaeser *et al*. (1985). A wet pellet containing 10 mg of PM was resuspended in 1.5 ml of 6% (w/v) sodium DOC at a pH of 8.8. After 18 hours the membranes were washed by centrifugation to form a band in a sucrose gradient, using 7% DOC to make up all solutions. The DOC was then removed from material in the band by dialysis against distilled water for three days followed by dialysis against 0.2% (w/v) azide for another three days. During dialysis the membranes were kept in the dark. Finally, the membranes were diluted with 50 ml distilled water, pelleted and resuspended in 1.5 ml of 0.2% azide.

Specimens of frozen-hydrated membranes on carbon film were prepared essentially as described by Subramaniam *et al*. (1993). However, when viewed in the electron microscope, grids prepared in this way showed membranes which were mostly rolled up and unsuitable for imaging. Flat membranes were obtained only when a drop of sodium acetate buffer at a pH of 4.5 was applied to the grids after blotting off the membrane suspension. Excess buffer was removed after 30 seconds and the grid was then frozen in liquid ethane.

Imaging was carried out on a Philips CM20 FEG fitted with a liquid helium-cooled objective lens (F.Z. & E.B., unpublished) running at 200 keV. Micrographs at 65,000 magnification were selected for strongest diffraction spots in the optical diffractometer and digitised at 7.5 μm per pixel (1.15 Å) over an area of 6000×6000 pixels on a Joyce-Lobl densitometer giving about 2.3 Å resolution cut-off. Seven micrographs were processed on a computer using the procedure described by Unwin & Henderson (1975) and Henderson *et al*. (1986).

Acknowledgements

The authors thank Richard Henderson, Joyce Baldwin and Per Bullough for their comments on the paper. This work was supported by EC grants ERBCHRX-CT94-0587 and ERBSCIX-CT91-0734 as well as MRC and Max Planck Gellschaft.

References

Baldwin, J. M., Henderson, R., Beckmann, E. & Zemlin, F. (1988). Images of purple membrane at 2.8 Å resolution obtained by cryo-electron microscopy. *J. Mol. Biol.* **202**, 585–591.

Blaurock, A. E. (1975). Bacteriorhodopsin: a trans-membrane pump containing α-helix. *J. Mol. Biol.* **93**, 139–158.

Blaurock, A. E. & Stoeckenius, W. (1971). Structure of the purple membrane. *Nature New Biol.* **233**, 152–155.

CRC Handbook of Chemistry and Physics (1978). (Weast, R. C., ed.), CRC Press, Cleveland.

Dubochet, J., Lepault, J., Freemann, C., Berriman, J. A. & Homo, J.-C. (1982). Electron-microscopy of frozen water and aqueous solutions. *J. Microsc.* **128**, 219–237.

Dubochet, J., Adrian, M., Chang, J.-J., Homo, J.-C., Lepault, J., McDowall, A. W. & Schultz, P. (1988). Cryo-electron microscopy of vitrified specimens. *Quart. Rev. Biophys.* **21**, 129–228.

Engleman, D. M., Henderson, R., Mclachlan, A. D. & Wallace, B. A. (1980). Path of the polypeptide in bacteriorhodopsin. *Proc. Natl Acad. Sci. USA*, **77**, 2023–2027.

Glaeser, R. M., Jubb, J. S. & Henderson, R. (1985). Structural comparison of native and deoxycholate-treated purple membrane. *Biophys. J.* **48**, 775–780.

Grigorieff, N. & Henderson, R. (1995). Diffuse scattering in electron diffraction data from protein crystals. *Ultramicroscopy*, in the press.

Havelka, W. A., Henderson, R., Heymann, J. A. W. & Oesterhelt, D. (1993). Projection structure of halorhodospin from *Halobacterium halobium* at 6 Å resolution obtained by electron cryo-microscopy. *J. Mol. Biol.* **234**, 837–846.

Henderson, R. (1975). The structure of the purple membrane from *Halobacterium halobium*: analysis of the X-ray diffraction pattern. *J. Mol. Biol.* **93**, 123–138.

Henderson, R. (1992). Image contrast in high-resolution electron microscopy of biological macromolecules: TMV in ice. *Ultramicroscopy*, **46**, 1–18.

Henderson, R. & Unwin, P. N. T. (1975). Three-dimensional model of purple membrane obtained by electron microscopy. *Nature*, **257**, 28–32.

Henderson, R., Jubb, J. S. & Whytock, S. (1978). Specific labelling of the protein and lipid on the extracellular surface of purple membrane. *J. Mol. Biol.* **123**, 259–274.

Henderson, R. Jubb, J. S. & Rossmann, M. G. (1982). A contracted form of the trigonal purple membrane of *Halobacterium halobium*. *J. Mol. Biol.* **154**, 501–514.

Henderson, R., Baldwin, J. M., Downing, K. H., Lepault, J. & Zemlin, F. (1986). Structure of purple membrane

from *Halobacterium halobium*: recording, measurement and evaluation of electron micrographs at 3.5 Å resolution. *Ultramicroscopy*, **19**, 147–178.

Henderson, R., Baldwin, J. M., Ceska, T. A., Zemlin, F., Beckmann, E. & Downing, K. H. (1990). Model for the structure of bacteriorhodopsin based on high-resolution electron cryo-microscopy. *J. Mol. Biol.* **213**, 899–929.

Hwang, S. B. & Stoeckenius, W. (1977). Purple membrane vesicles: morphology and proton translocation. *J. Membrane Biol.* **33**, 325–350.

International Tables of Crystallography (1992). (Wilson, A. J. C., ed.), vol. C, Kluwer Academic Publishers, Dordrecht.

Karrasch, S., Bullough, P. A. & Ghosh, R. (1995). The 8.5 Å projection map of the light-harvesting complex I from *Rhodospirillum rubrum* reveals a ring composed of 16 subunits. *EMBO J.* **14**, 631–638.

Kates, M., Kushwaha, S. C. & Spott, G. D. (1982). Lipids of purple membrane from extreme halophiles and of methanogenic bacteria. *Methods Enzymol.* **88**, 98–111.

Schertler, F. R. X., Villa, C. & Henderson, R. (1993). Projection structure of rhodopsin. *Nature*, **362**, 770–772.

Sternberg, B., L'Hostis, C., Whieway, C. A. & Watts, A. (1992). The essential role of specific *Halobacterium halobium* polar lipids in 2D-array formation of bacteriorhodopsin. *Biochim. Biophys. Acta*, **1108**, 21–30.

Subramaniam, S., Gerstein, M., Oesterhelt, D. & Henderson, R. (1993). Electron diffraction analysis of structural changes in the photocycle of bacteriorhodopsin. *EMBO J.* **12**, 1–8.

Szundi, I. & Stoeckenius, W. (1987). Effect of lipid surface charges on the purple-to-blue transition of bacteriorhodopsin. *Proc. Natl Acad. Sci. USA*, **84**, 3681–3684.

Szundi, I. & Stoeckenius, W. (1988). Purple-to-blue transition of bacteriorhodopsin in a neutral lipid environment. *Biophys. J.* **54**, 227–232.

Tanford, C., Nozaki, Y., Reynolds, J. A. & Makino, S. (1974). Molecular characterization of proteins in detergent solutions. *Biochemistry*, **11**, 2369–2376.

Tsygannik, I. N. & Baldwin, J. M. (1987). Three-dimensional structure of deoxycholate-treated purple membrane at 6 Å resolution and molecular averaging of three crystal forms of bacteriorhodopsin. *Eur. Biophys. J.* **14**, 263–272.

Unwin, P. N. T. & Henderson, R. (1975). Molecular structure determination by electron microscopy of unstained crystalline specimen. *J. Mol. Biol.* **94**, 425–440.

Wade, R. H. (1992). A brief look at imaging and contrast transfer. *Ultramicroscopy*, **46**, 145–156.

Zaccai, G. & Gilmore, D. J. (1979). Areas of hydration in the purple membrane of *Halobacterium halobium*: A neutron diffraction study. *J. Mol. Biol.* **132**, 181–191.

Edited by A. Klug

(Received 9 June 1995; accepted 25 September 1995)